NDT and E International 102 (2019) 120–128

Contents lists available at ScienceDirect

NDT and E International

journal homepage: www.elsevier.com/locate/ndteint

Automated visualization of concrete bridge deck condition from GPR data

Kien Dinh[a,*], Nenad Gucunski[b], Tarek Zayed[c]

[a] CONSEN Inc, Montréal, Canada
[b] Department of Civil & Environmental Engineering, Rutgers University, NJ, USA
[c] Department of Building and Real Estate (BRE), The Hong Kong Polytechnic University, Hong Kong

ARTICLE INFO

Keywords:
Concrete
Corrosion
Ground-penetrating radar
Nondestructive evaluation
Condition assessment
Bridge inspection
Automation

ABSTRACT

Ground-penetrating radar (GPR) is one of the most commonly used technologies for condition assessment of concrete bridge decks. However, there have been no fully automated algorithms to visualize the data collected with this technique. In such context, the current paper presents a method for a full automation of GPR data visualization and analysis. Based on the background removal, depth correction, synthetic aperture focusing technique (SAFT), and interpolation algorithms, this automated method produces a plan view map of amplitude of GPR signals. In the obtained map, two types of information are observed at the same time. First, as the strongest reflectors of electromagnetic energy, rebars will appear as the most visible. Second, the areas of corrosive environment and, thus, likely corrosion, will be detected as having low amplitude rebar reflections. As a proof of concept, the proposed method was implemented for two bare concrete bridge decks and two concrete bridge decks with asphalt overlays. In all cases, the results obtained were excellent where the maps pinpointed the areas affected by corrosion. These areas were confirmed by other methods of evaluation, such as electrical resistivity (ER), half-cell potential (HCP), chloride analysis of core samples, or visual inspection. With the demonstrated performance, the proposed method is expected to be an excellent alternative to the available methods of GPR data evaluation and visualization. In the future, it should be improved to provide an indication of corrosion severity/probability at each deck location.

1. Introduction

Ground-penetrating radar (GPR) is one of the most effective technologies for concrete bridge deck inspection [1]. It has been successfully used to capture concrete deck deterioration progression [2] and has been integrated into an advanced robotic nondestructive evaluation (NDE) platform [3]. Based on principles of electromagnetic (EM) wave propagation, the GPR employs antennas to transmit a short pulse of EM energy and receive the reflected signals. For each survey location, the received waveforms are recorded in the time domain to form what is called an A-scan signal. A raw B-scan is created by stacking all A-scans collected for the same test line. To a certain extent, a raw B-scan represents a cross-section of the structure being surveyed. It is noted, however, that a more accurate representation should be obtained through the process of image reconstruction, which will be described in more detail in the research methodology section.

As an EM waves based method, the GPR is mainly employed to evaluate material properties and processes influenced by changes in dielectric and electrical conductivity [4]. For concrete bridge decks, those properties indicate corrosive environment, because the co-presence of moisture, chloride ions, rust (iron oxide) will affect GPR signals [1]. Separately, while the main effects of moisture are to slow down the propagation of GPR signals and give rise to a dielectric loss, the electric charges of the freely moving ions will induce eddy currents and, consequently, lead to a conductive loss of the EM energy [5]. Considering these characteristics of GPR, the bridge deck condition will be understood hereafter as related to the development and severity of corrosive environment. Certainly, the severity of the corrosive environment will increase as concrete deteriorates, with forming of cracks and delamination, and the increase of concentration of moisture, chlorides, and others consequently.

With respect to the analysis of GPR data from concrete bridge deck surveys, many approaches have been proposed in the literature [4–12]. While most of these approaches are based on the analysis of amplitudes of reflection, Tarussov et al. [4] argued that a visual interpretation by an experienced GPR analyst would provide much more accurate evaluations. To justify their claim, the authors pointed out three specific reasons. First, they view the GPR as an imaging device and not a measuring instrument. Second, they stated that a simple analysis of amplitude would ignore most information contained in the B-scans, and

* Corresponding author.
E-mail addresses: kien.dinh@consen.ca (K. Dinh), gucunski@soe.rutgers.edu (N. Gucunski), tarek.zayed@polyu.edu.hk (T. Zayed).

https://doi.org/10.1016/j.ndteint.2018.11.015
Received 11 June 2018; Received in revised form 15 October 2018; Accepted 22 November 2018
Available online 23 November 2018
0963-8695/ © 2018 Elsevier Ltd. All rights reserved.

that such an analysis can be affected by many factors, such as the rebar depth, surface anomalies, rebar configuration, polarization effects, etc. Finally, the authors explained the issue with the conventional method of contour mapping. According to them, as this method was based on interpolation, it was not suitable to map corroded areas, which usually had sharp limits in B-scans.

Whereas the aforementioned authors provided a good discussion on the limitations of the conventional contour mapping method, there should be no question regarding whether GPR is a measuring or imaging technique. To clarify, an image itself is created by many pixel elements that differentiate from each other by the so-called intensity values, which are numbers. Therefore, ultimately, what can be seen in an image are completely governed by the numbers representing the image pixels. In other words, the intensity values can be processed to obtain the information contained in digital images. This has been the foundation of computer vision, a scientific discipline with many outstanding recent achievements.

It is agreed with the above authors that the conventional amplitude method does not fully exploit the information contained in the GPR data and provides a limited visualization of the condition of bridge decks. From the start of this research, it was hypothesized that the use of synthetic aperture focusing technique (SAFT) would not only provide a clear vision of rebar locations, but would also help visualize the corrosion affected areas. In the literature, this technique has been successfully used to restore ultrasonic images with focusing distortion [13,14]. For civil engineering applications, it has been used to process ultrasonic data from concrete structures [15–18]. For an unknown reason, while this technique can be used to evaluate the condition of concrete bridge decks from GPR signals, its application has been limited only to concrete imaging problems [19,20]. Gucunski et al. [21] presented visualization of GPR survey results. The presented visualization of the bridge deck condition was done through time slicing of unmigrated GPR signals. The shortcoming of time slicing approach is that a time slice view is not able to include all the rebars, if those are at different depths. In addition, time slicing of unmigrated data will not provide a clear plan view of a bridge deck with focused energies.

With such a study hypothesis, the ultimate goal of this research was to develop a method for better visualization and analysis of a concrete bridge deck condition by GPR. The expectation of the method was twofold. First, that it would enable a fully automated visualization of bridge deck GPR data. Second, that a comprehensive visualization would improve the accuracy of GPR data evaluation. Related to the first expectation, while significant developments have been made with respect to automated rebar picking [22–25], it was reported that the picking accuracy was reduced for deck areas with highly attenuated GPR signals [24]. That is to say, the reliability of deck evaluation based on automated rebar picking methods might be compromised for concrete bridge decks with severe deterioration.

2. Research methodology and model development

As depicted in Fig. 1, the methodology proposed in this research is based upon very simple ideas. First, as a nearly perfect reflector of radio-frequency EM energy, steel bars will produce the strongest reflections, compared to other material interfaces in the deck system. Thus, a plan view map of the amplitude data should completely unveil rebar locations. In addition, the map should also reveal other surface objects such as deck joint, drain grate, or amplitude anomalies caused by factors unrelated to deterioration. Second, like the conventional method, it will be possible to evaluate the condition of a bridge deck through comparing the amplitudes between different areas of the deck. With respect to the effects of rebar depth variation, they can be accounted for in the final amplitude map by applying a depth correction (gain) function before the reconstruction of B-scans. Each of the steps in Fig. 1 will be described in detail in the following subsections.

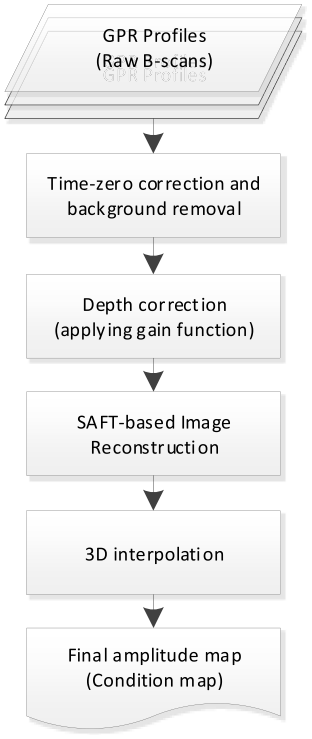

Fig. 1. Procedure for visualizing GPR data from concrete bridge decks.

2.1. Time-zero correction and background removal

The zero time is defined corresponding to the reflection from the ground surface [24,25]. An accurate selection of zero time is therefore important in analyzing GPR images. However, while the surface reflections from an air-horn antenna are evident, due to their mixture with the direct wave, those from ground-coupled GPR are not obvious. As a result, an accurate determination of zero time will usually require an appropriate equipment setup and calibration. Since such a calibration was not performed in this study, the zero time suggested in a previous research [26] was utilized. More specifically, the zero time is located at 0.61 ns before the first positive peak of each A-scan on GPR images. Because this position might be slightly different between A-scans in the same image due to different reasons, the mean value position is employed in this research for each B-scan.

As mentioned above, the first wavelet in an A-scan is associated with the ground surface. For a ground-coupled antenna, this wavelet is mixed with the direct wave between transmitter and receiver to form what is called a direct-coupling reflection [5,12]. For concrete bridge decks, these reflections are usually very strong, comparable to the reflections from the top reinforcing layer. Therefore, if they are not properly removed, one might not be able to see the reflections from rebars in the plan view mode. It was realized that a background removal technique would be able to address this problem [27]. Additionally, the background removal will also help remove the ringing noise that might affect GPR data analysis results for thick structures [28]. More specifically, a mean subtraction method is employed in this research for the background removal. Mathematically, the method can be described in Equation (1). An example of B-scan for a concrete deck before and after the background removal, as the first processing step, is provided in Fig. 2.

$$S_{br}^{i}(t) = S_{r}^{i}(t) - \frac{\sum_{j=1}^{N} S_{r}^{j}(t)}{N} \quad (1)$$

Where:

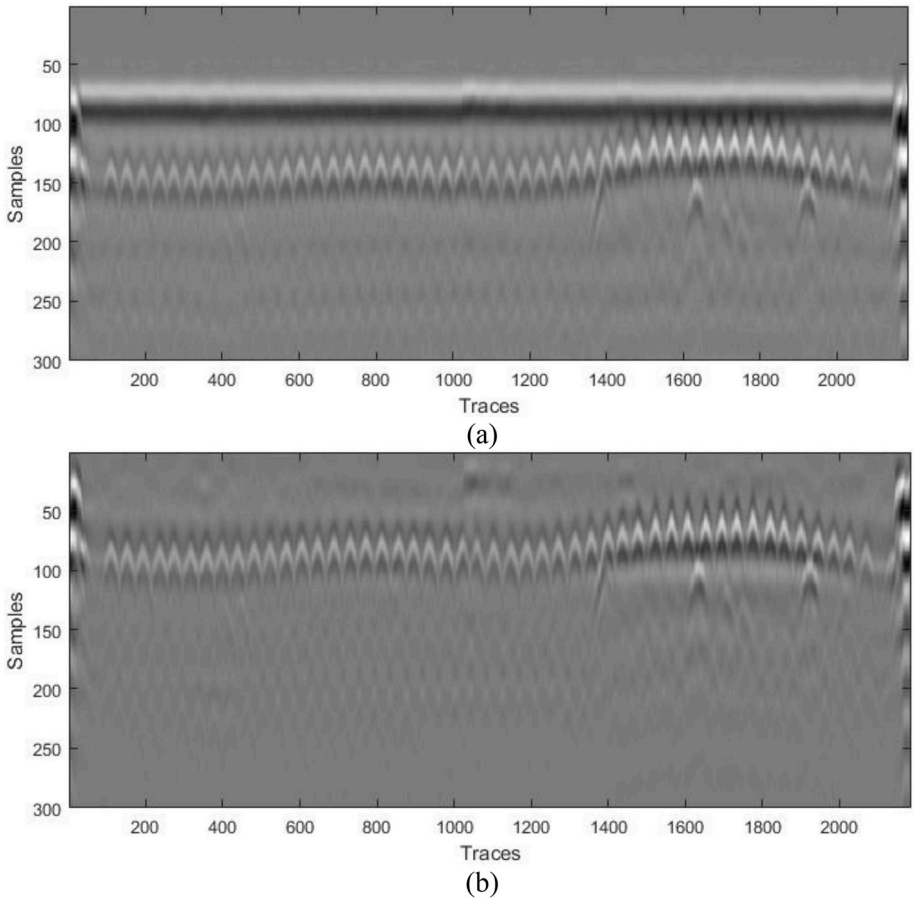

Fig. 2. (a) Raw profile and (b) After time-zero correction and background removal.

$S_r^i(t)$: Signal amplitude of A-scan number i at time t
$S_{br}^i(t)$: Signal amplitude of A-scan number i at time t after background removal
N: Number of A-scans on the GPR profile

2.2. Depth correction

The effects of concrete cover thickness (rebar depth) variation on the reflection amplitude have been studied and well understood [5,8]. Therefore, those have been accounted for in the conventional method of amplitude evaluation [5]. Similarly, to consider those effects in the proposed methodology, a gain function is employed. The gain function should describe the relationship between the rebar depth and amplitude of reflection for a sound concrete only. Once the GPR signals have been adjusted with such a function, one should expect that the reflections from rebars in a sound concrete deck would have approximately the same amplitude values. As the needed gain function has been found in the literature [5] for the antennas of the same frequency to those employed in this research, it was simply adopted. Equation (2) explains the use of gain function to adjust the amplitude values of each A-scan. Fig. 3 illustrates the effects of this step where it shows exactly the same B-scan in Fig. 2b, but after being adjusted by the adopted gain function. As can be seen, the amplitude variation due to the difference in rebar depth has been minimized.

$$S_g^i(t) = S_{br}^i(t) \times G(t) \tag{2}$$

Where:

$S_{br}^i(t)$: Signal amplitude of A-scan number i at time t after background removal
$S_g^i(t)$: Signal amplitude of A-scan number i at time t after applying gain function G
$G(t)$: Value of gain function G at time t

2.3. SAFT-based image reconstruction

SAFT is a powerful technique for analyzing ultrasonic and GPR signals. As described in Equation (3), it is based on projecting each individual A-scan in the synthetic aperture to the evaluated cross section and then superimposing the results of all A-scans. To illustrate the results of SAFT algorithm application, a section of B-scan reconstructed from the GPR profile in Fig. 3 is provided in Fig. 4. It is noted that this section corresponds to the first portion of the GPR profile and therefore the ringing effects from the steel deck joint are visible. From the B-scan, it is evident that the gain function applied in the previous step has created intended effects. More specifically, the bottom rebars can be clearly seen and their amplitudes are comparable to those of the top rebars. Related to this observation, while the shadows of the top rebars can also be noticed between the two layers of steel reinforcement, they should not be misunderstood as an additional rebar layer. With respect to the most important parameter used for the image reconstruction, based on the previous studies [24,25], a GPR signal velocity of 0.1 m/ns has been utilized.

$$A(x, d) = \sum_{i=1}^{N} S_g^i\left(t = \frac{L^i}{V}\right) \tag{3}$$

Where:

$A(x, d)$: Amplitude of a pixel in the reconstructed B-scan at distance x and depth d
$S_g^i(t)$: Signal amplitude of A-scan number i at time t after applying

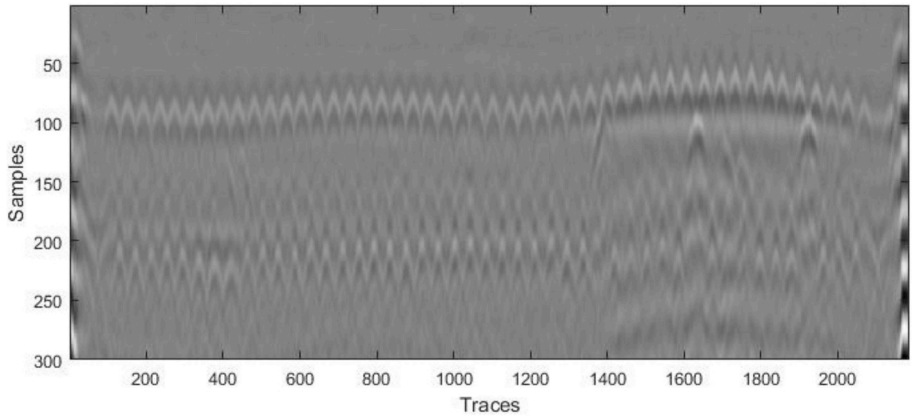

Fig. 3. Depth-corrected B-scan.

gain function G

L^i: Travel length of the signal corresponding to A-scan number i from the transmitter to the pixel and back to the receiver.

V: Signal velocity

N: Number of A-scans in the GPR profile (synthetic aperture)

Compared to other migration techniques for GPR data, the SAFT offers two major advantages as follows. The first and most important, it allows the projected cross section areas and their resolution to be selected independently from the collected B-scans. Therefore, with the SAFT algorithm, one would not need to scale or cut GPR profiles to make sure that all of them have the same resolution, or to start and end at the same transverse lines. This requirement is important for three-dimensional (3D) image reconstruction that involves an interpolation of two-dimensional (2D) matrices of the same size. Second, since each A-scan is projected sequentially to the evaluated cross section, the technique enables the possibility of real time processing of GPR signals [19].

2.4. 3D interpolation

A condition map is, in most cases, the desired output from a GPR survey of concrete bridge deck. Similar to the conventional amplitude method, in this study, an interpolation will be employed to transform the amplitude data obtained from GPR profiles to a plan view map of a bridge deck. However, unlike the conventional method that uses only a portion of data acquired from the rebar-picking step, the proposed method will employ the entire amplitude data in the B-scans reconstructed with the SAFT technique. More specifically, a linear 3D interpolation technique will be utilized to obtain the missing amplitude data between the B-scans and create a 3D model of the concrete bridge deck being surveyed. Finally, the condition map will be generated by simply taking the plan view of that 3D model. An example output of this step is provided in Fig. 5 for a small section of a concrete bridge deck. As can be seen, the maps obtained this way clearly indicate the rebar locations. More importantly, as will be seen in the subsequent case studies, the maps obtained using this method will pinpoint the corrosion-affected areas.

3. Case study implementation

As one might realize, the above procedure does not involve any manual processing of GPR data and, therefore, it enables a fully automated visualization of concrete bridge deck condition. Specifically, a program with built-in 3D interpolation functions has been written in MATLAB to fully automate the proposed methodology. In this section, the MATLAB program is employed to visualize the condition of four bridge deck cases. Two cases are bare concrete bridge decks in the US, while the other two are concrete bridge decks with asphalt overlays in Canada. For a validation, the results obtained will be compared to those acquired using other evaluation methods, such as electrical resistivity (ER), half-cell potential (HCP), coring and visual inspection. It is noted that, all the GPR surveys were conducted using 1.5-GHz ground-coupled antennas manufactured by Geophysical Survey Systems, Inc. (GSSI).

3.1. Elkton Bridge, Maryland, United States

The Elkton Bridge, which crosses over Little Elk Creek in Maryland, was constructed in 1973. The bridge consists of a bare concrete deck supported by seven steel girders, two abutments and a middle pier. The deck is 27 m long and 14 m wide, with a thickness of 20 cm and a skew angle of $14^0 53'$. To evaluate corrosion, the deck was tested in July 2013 using three NDE techniques, namely GPR, HCP and ER. The HCP and ER data were collected on a 0.6 m × 0.6 m grid, while the GPR scan lines were set up parallel to the traffic with a 0.6 m spacing. The GPR scan lines completely matched the survey grid of the other two technologies in the traffic direction.

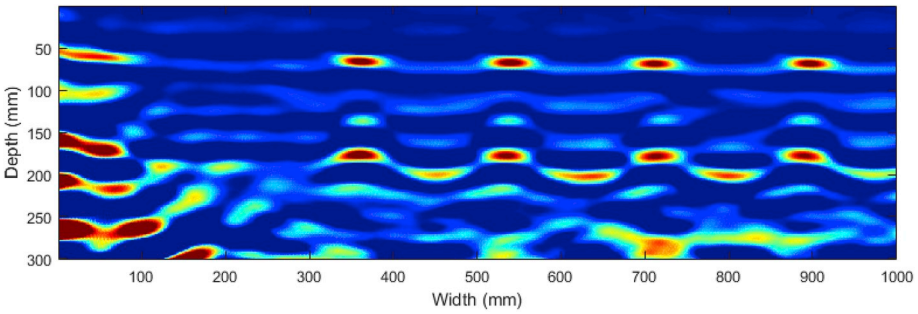

Fig. 4. B-scan reconstructed using SAFT.

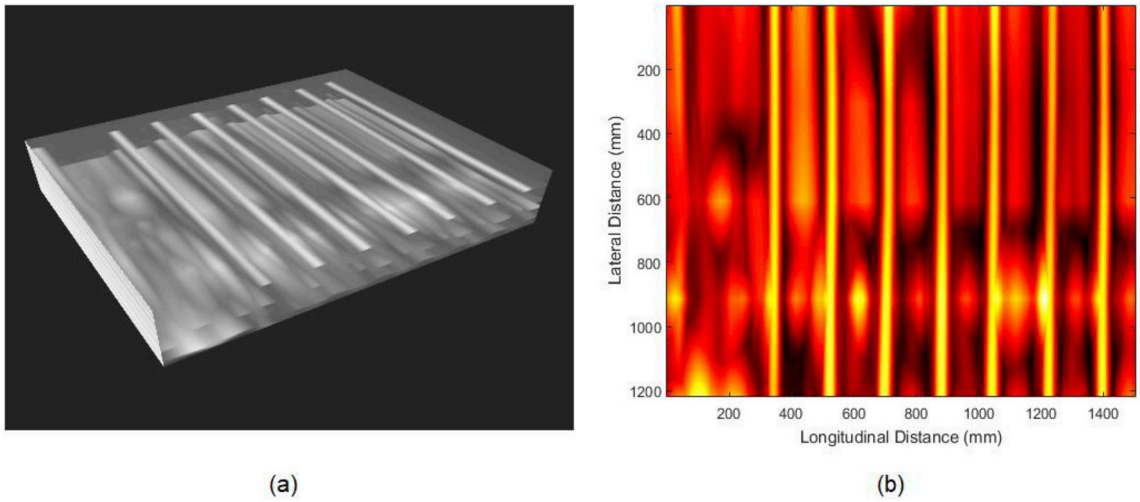

Fig. 5. (a) Interpolated 3D model and (b) plan view amplitude map.

Fig. 6 presents the test results for the three NDE technologies. As can be seen, the areas of low amplitude on the map developed from GPR closely match with areas of low electrical resistivity by ER and high probability for corrosion activity by HCP. Since all the amplitude data on the original profiles are used, compared to the other two techniques, the GPR map provides a much greater level of detail. More specifically, it depicts the reinforcement position, the areas of likely corrosion associated with each rebar, along with the locations of deck joint. However, a limitation of such a GPR map is that it does not indicate numerically the severity of corrosion/deterioration. The only symptom one can use is that, the rebars will tend to disappear in the areas of severe corrosion, while those in slightly corrosive regions will be manifested by moderate amplitude values.

3.2. Pequea Bridge, Pennsylvania, United States

The Pequea Bridge was built in 1970 in Conestoga, Pennsylvania. It is of the same structure type as the Elkton Bridge, i.e., a bare concrete deck on steel girders. The deck of the bridge was surveyed in August 2013 using the same NDE equipment and setup as the Elkton Bridge. The test results are provided in Fig. 7. As can be observed again, the GPR map clearly indicates the areas likely affected by corrosion anticipated by the ER and HCP. While one might notice a better correlation between GPR and ER test results than the one between the GPR and HCP results, this is not surprising since electrical conductivity of concrete is the primary factor affecting the electrical resistivity and EM wave attenuation.

3.3. Bridge X, Quebec, Canada

Bridge X, situated in Laval, Quebec, Canada, was constructed in 1966. It consisted of a reinforced concrete deck supported by five steel girders. The deck was overlaid with an asphalt layer of average 7 cm thick. The thickness of the concrete slab was 30 cm. Since severe corrosion-induced damages could be seen on the deck soffit, the Ministry of Transportation of Quebec (MTQ) decided that the deck would be demolished and replaced in 2014. Before the demolition, several tests were performed to study the bridge deck condition. With respect to corrosion, the tests performed included the GPR, HCP and chloride content analysis of core samples. Unlike the first two bridge decks, the GPR data was collected more densely, with a 0.3 m spacing, while the HCP test was performed on a 1 m × 1 m grid. To ensure an electrical connectivity between the HCP electrode and the concrete surface, small holes were drilled through the asphalt layer at the test locations. Fig. 8 shows the test results from the GPR and HCP surveys. It should be noted that, since the HCP map was developed by an independent engineering consulting group, its color legends are not the same as the HCP maps depicted in the previous case studies.

As can be seen, the first impression from the two maps is that they highly correlate with each other. The dark color on the two maps suggest the areas of likely severe corrosion. In addition, the voltage measurements on the HCP map indicate that, at the time when the test was performed, it was very likely that the entire deck area had active corrosion. This possibility is confirmed by the results from chloride analysis of core samples shown in Table 1. Specifically, all the chloride concentrations measured from the cores exceed 0.025%, the commonly accepted threshold that might initiate rebar corrosion [29]. From the maps and the table, one might also notice the effects of chloride content on the GPR and HCP measurements. The higher the chloride content, the more attenuated the GPR signals and the lower (more negative) the HCP voltage value.

3.4. Bridge Y, Quebec, Canada

Bridge Y, located in Montreal, Quebec, Canada carries a two-way traffic in East-West direction. The Eastbound and Westbound lanes are separated from each other by a median strip of 1.2 m wide. The bridge deck is 36.5 m long and 45 cm thick, with an asphalt overlay. Like in the case of Bridge X, the GPR scan lines were set up parallel to the traffic with a 0.3 m spacing distance. In addition to the GPR survey, the deck soffit was inspected visually. The results are presented in Fig. 9 for both methods of evaluation.

As can be seen, the GPR amplitude map in Fig. 9a clearly shows the positions of drain grates on the deck, along with the rebar locations. Since those grates were made from steel, they produced strong reflections in GPR data. With respect to corrosion, as the areas of likely corrosive environment absorb more EM energy than those of sound concrete, they are manifested as the regions of low amplitude rebar reflection. For a comparison with the results from visual inspection, some of these areas are numbered on the GPR map. A close match between those areas and the spalling defects in Fig. 9b can be observed. Based on the defect locations, it is very likely that the water and deicing salts from the drainage system had caused major deterioration of the bridge deck in this case.

4. Discussion

While the case studies have clearly illustrated the implementation of the proposed methodology, this section discusses some issues, parameters, and effects of interest in applying the developed algorithm. It is

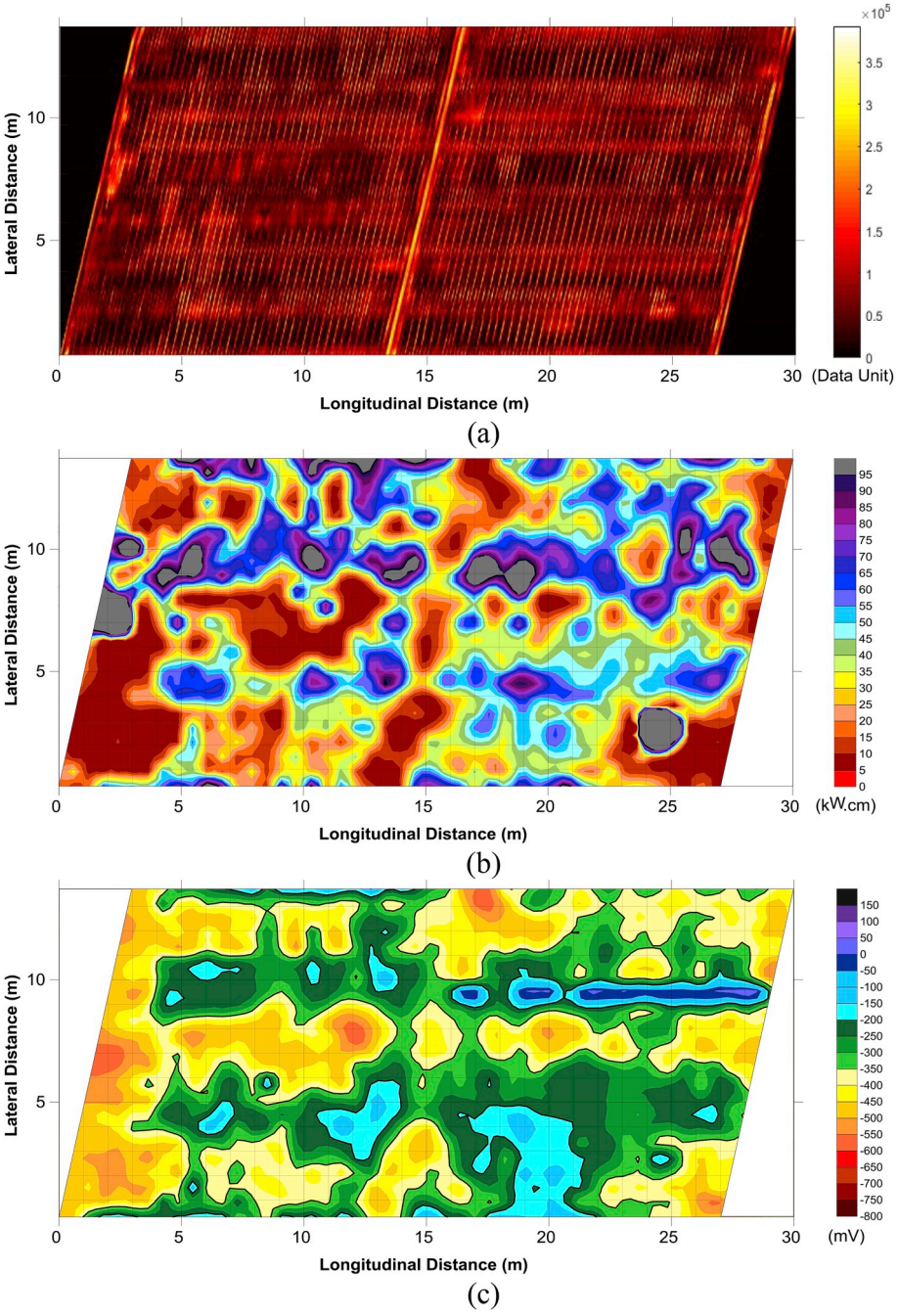

Fig. 6. Condition maps for the Elkton Bridge deck: (a) the proposed method for GPR data, (b) ER and (c) HCP.

not expected that the presented method will be effective in visualization of GPR data collected with an air-coupled antenna. The reason is that the reflections from rebar mats will appear in B-scans more as a layer, rather than individual rebars. Therefore, the SAFT algorithm will likely be ineffective in resolving the described resolution problem.

First, a false estimation of zero time in the first step may lead to errors in identifying the rebar depth information. Specifically, if the first positive peak of an A-scan is taken as a reference, and the same signal velocity is used in the third step of the algorithm, a more negative value of the zero time will make a rebar to appear deeper after performing the SAFT operation. Thus, a limitation of the current study is that the zero time was adapted from the literature [26], in which a different GPR equipment might have been used.

Second, it is worthy to note that the gain function employed in this study was developed from a large library of GPR signals collected on many sound concrete decks [5]. The purpose of the gain function was to eliminate the effects of beam scattering and dielectric loss to achieve the following. If one compares the reflection amplitudes of two rebars in a sound concrete deck, those amplitudes will be approximately equal after the gain function application, even when they have different concrete cover thickness. As another note, unlike a commonly understood gain function, which is utilized to amplify or diminish the GPR signals; the ultimate goal of the gain function in this research is to compensate for the signal loss due to an increase in concrete cover thickness.

It might be reasonable to assume a different signal velocity for each surveyed deck, and in the SAFT algorithm, due to a variation of moisture content. However, an examination of GPR data for a large number of bridge decks has shown that a signal velocity of 0.1 m/ns is close to the actual velocities in most cases. Specifically, when this value

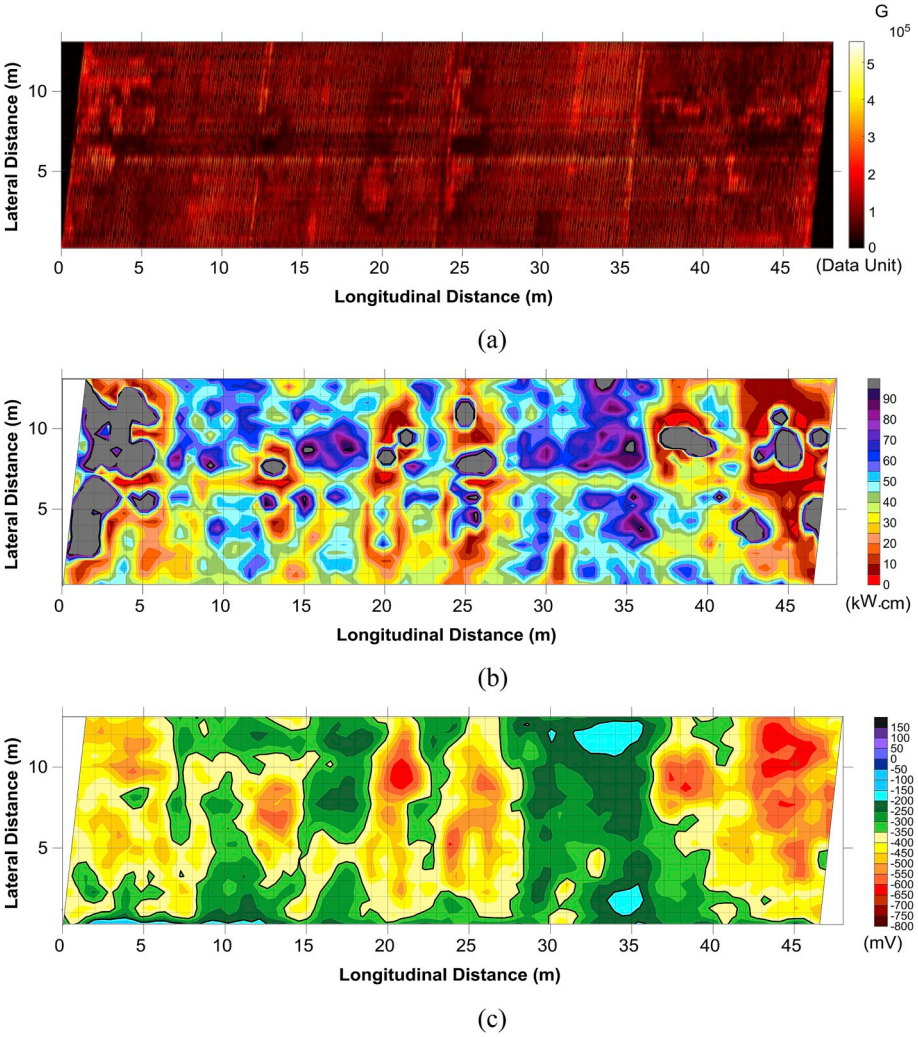

Fig. 7. Condition maps for the Pequea Bridge deck: (a) the proposed method for GPR data, (b) ER and (c) HCP.

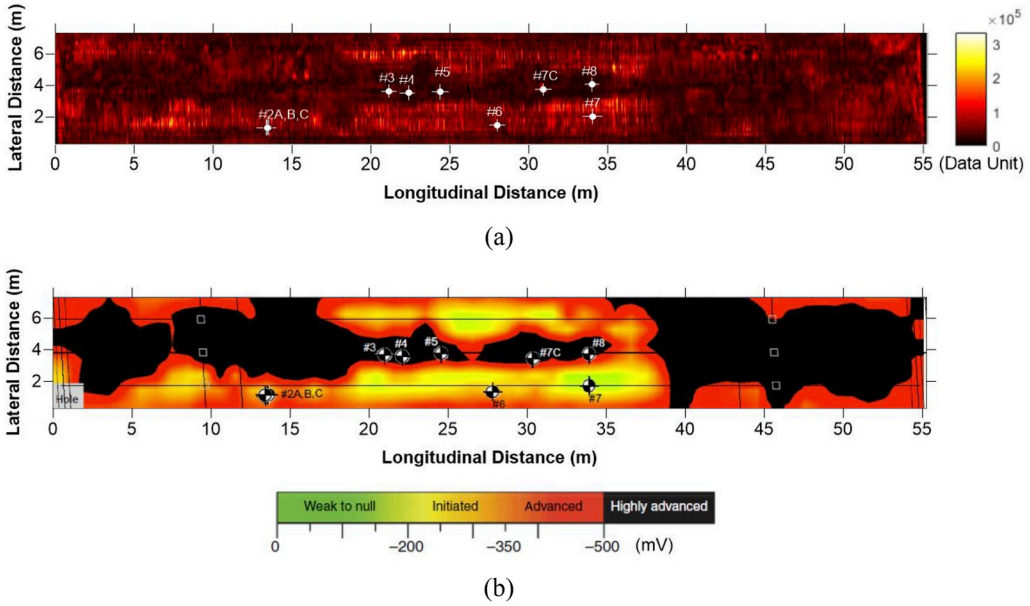

Fig. 8. Condition map of bridge deck X: (a) the proposed method and (b) HCP.

Table 1
Chloride analysis of core samples for Bridge X.

Core #	Chloride ion content (% mass of concrete)		
	At 0–20 mm	At 30–50 mm	At 60–80 mm
2A	–	–	–
2B	–	–	–
2C	–	–	–
3	–	–	–
4	–	–	–
5	0.310	0.271	0.155
6	0.037	0.040	0.049
7	0.124	0.136	0.091
7C	–	–	–
8	0.567	0.338	–

Note: indicates data not available.

was used in the migration, all the hyperbolic signatures of rebars were collapsed to point-like objects without the observable effects of under- or over-migration [24]. It means that the assumed value of 0.1 m/ns is acceptable and will not have a significant effect on the visualization of deck condition.

The case studies presented later point to a good correlation between GPR, ER and HCP results. The correlation can be explained in the following way. The GPR is an appropriate tool to describe the corrosive environment, which is primarily controlled by the electrical conductivity of concrete [1,4,5]. The ER is an NDE technology that is directly influenced by the same parameter [30]. On the other hand, the HCP is a technique that evaluates the probability of rebar active corrosion [1]. An expectation that the rebar corrosion will be initiated and supported by a corrosive environment explains, thus, a good correlation between the three technologies.

Finally, it is reasonable to expect some effects of the asphalt overlay on the deck condition visualization. In an ideal case, where the thickness of the overlay and the reflection amplitude at the asphalt/concrete interface are constant over the length of B-scans, there will be no effects on the visualization. This is because the reflection amplitude at the asphalt/concrete interface will be removed after the background removal operation. On the other hand, if either the overlay thickness or the reflection amplitude at the asphalt/concrete interface vary over the length of a GPR profile, one should observe some effects on the condition map obtained from the proposed methodology. Specifically, in addition to the strongest reflections from rebars, one could see a few bright areas in the amplitude map as a result of the asphalt/concrete

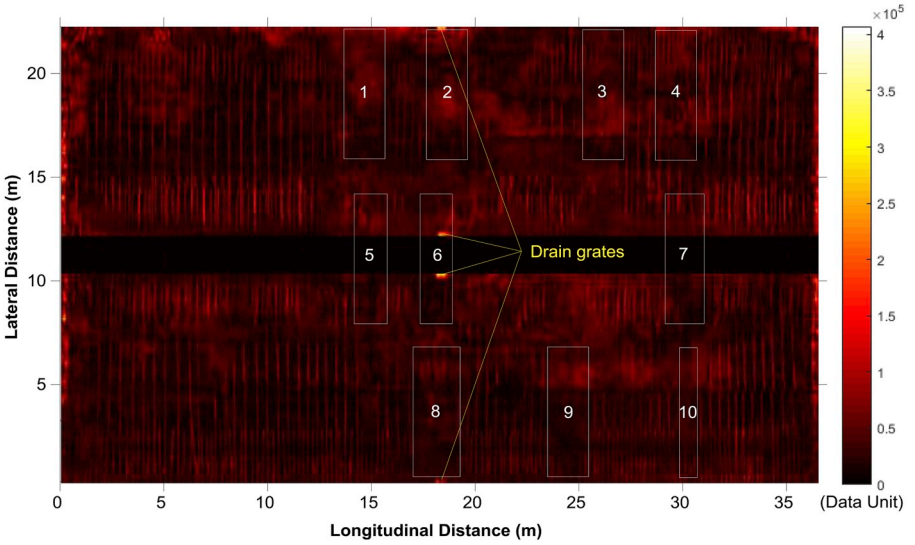

(a)

(b)

Fig. 9. Assessment of bridge deck Y: (a) GPR and (b) visual inspection of slab bottom.

interface reflection. However, since those reflections usually have a much smaller amplitude than those from rebars, the effects will not be significant. This was illustrated in the condition maps for the two bridge decks with asphalt overlays. Specifically, in the condition maps for the two bare concrete decks, only bright colors appear at rebar locations. On the other hand, some bright, cloudy areas can be observed in the condition maps for the decks with asphalt overlays. This is because some reflections from the asphalt/concrete interface were not eliminated through the background removal.

5. Conclusions

Automated analysis of GPR data for concrete bridge decks is a challenging task that has led to many efforts to achieve it. Most of those efforts have been directed toward the automation of rebar picking, the most time consuming step in the conventional method of amplitude evaluation. By integrating the background removal, depth correction, SAFT and interpolation algorithms, a new and fully automated method was developed in this study to visualize the concrete bridge deck condition from GPR data. Expressed in the form of an amplitude map, the final output of the method for a bridge deck provides two important pieces of information. First, it presents the locations of rebars and other surface objects such as deck joints or drain grate, etc. Second, it pinpoints the areas of likely corrosive environment. The method was successfully implemented and the results validated on the decks of four bridges in the US and Canada. In all cases, the GPR maps clearly visualized the locations of rebar objects and the areas of reinforced concrete corrosion. These areas were verified by other methods of deck evaluation, such as ER, HCP, chloride analysis of core samples, or visual inspection.

Acknowledgements

The authors are grateful to the US Federal Highway Administration (FHWA), Long Term Bridge Performance (LTBP) Program, Ministry of Transportation of Quebec (MTQ), Mitacs and Radex Detection Inc. for their support during the course of this study.

Appendix A. Supplementary data

Supplementary data to this article can be found online at https://doi.org/10.1016/j.ndteint.2018.11.015.

References

[1] Gucunski N, Imani A, Romero F, Nazarian S, Yuan D, Wiggenhauser H, et al. Nondestructive testing to identify concrete bridge deck deterioration. Washington D.C: Transportation Research Board; 2013. https://doi.org/10.17226/22771.
[2] Gucunski N, Pailes B, Kim J, Azari H, Dinh K. Capture and quantification of deterioration progression in concrete bridge decks through periodical NDE surveys. J Infrastruct Syst 2016 Jun 17;23(1):B4016005. https://doi.org/10.1061/(ASCE)IS.1943-555X.0000321.
[3] Gucunski N, Basily B, Kim J, Jin GY, Duong T, Dinh K, et al. RABIT: implementation, performance validation and integration with other robotic platforms for improved management of bridge decks. International Journal of Intelligent Robotics and Applications 2017 Jul 17;1(3):271–86. https://doi.org/10.1007/s41315-017-0027-5.
[4] Tarussov A, Vandry M, De La Haza A. Condition assessment of concrete structures using a new analysis method: ground-penetrating radar computer-assisted visual interpretation. Construct Build Mater 2013;38:1246–54. https://doi.org/10.1016/j.conbuildmat.2012.05.026.
[5] Dinh K, Gucunski N, Kim J, Duong TH. Understanding depth-amplitude effects in assessment of GPR data from concrete bridge decks. NDT E Int 2016 Oct 31;83:48–58. https://doi.org/10.1016/j.ndteint.2016.06.004.
[6] Chung T, Carter CR, Masliwec T, Manning DG. Impulse radar evaluation of asphalt-covered bridge decks. IEEE Trans Aero Electron Syst 1992 Jan;28(1):125–37. https://doi.org/10.1109/7.135439.
[7] Barnes CL, Trottier JF. Effectiveness of ground penetrating radar in predicting deck repair quantities. J Infrastruct Syst 2004 Jun;10(2):69–76. https://doi.org/10.1061/(ASCE)1076-0342(2004)10:2(69).
[8] Barnes CL, Trottier JF, Forgeron D. Improved concrete bridge deck evaluation using GPR by accounting for signal depth–amplitude effects. NDT E Int 2008 Sep 30;41(6):427–33. https://doi.org/10.1016/j.ndteint.2008.03.005.
[9] Martino N, Maser K, Birken R, Wang M. Quantifying bridge deck corrosion using ground penetrating radar. Res Nondestr Eval 2016 Apr 2;27(2):112–24. https://doi.org/10.1080/09349847.2015.1067342.
[10] Dinh K, Zayed T, Moufti S, Shami A, Jabri A, Abouhamad M, et al. Clustering-based threshold model for condition assessment of concrete bridge decks with ground-penetrating radar. Transport Res Rec: Journal of the Transportation Research Board 2015 Aug 1(2522):81–9. https://doi.org/10.3141/2522-08.
[11] Dinh K, Zayed T, Romero F, Tarussov A. Method for analyzing time-series GPR data of concrete bridge decks. J Bridge Eng 2014;20(6). https://doi.org/10.1061/(ASCE)BE.1943-5592.0000679. 04014086.
[12] Dinh K, Gucunski N, Kim J, Duong TH. Method for attenuation assessment of GPR data from concrete bridge decks. NDT E Int 2017 Dec 1;92:50–8. https://doi.org/10.1016/j.ndteint.2017.07.016.
[13] Langenberg KJ, Berger M, Kreutter T, Mayer K, Schmitz V. Synthetic aperture focusing technique signal processing. NDT Int 1986;19.3:177–89. https://doi.org/10.1016/0308-9126(86)90107-0.
[14] Spies M, Rieder H, Dillhöfer A, Schmitz V, Müller W. Synthetic aperture focusing and time-of-flight diffraction ultrasonic imaging—past and present. J Nondestr Eval 2012;31:310–23. https://doi.org/10.1007/s10921-012-0150-z.
[15] Schickert M, Krause M, Müller W. Ultrasonic imaging of concrete elements using reconstruction by synthetic aperture focusing technique. J Mater Civ Eng 2003;15:235–46. https://doi.org/10.1061/(ASCE)0899-1561(2003)15:3(235).
[16] Krause M, Milmann B, Mielentz F, Streicher D, Redmer B, Mayer K, et al. Ultrasonic imaging methods for investigation of post-tensioned concrete structures: a study of interfaces at artificial grouting faults and its verification. J Nondestr Eval 2008 Sep 1;27(1–3):67–82. https://doi.org/10.1007/s10921-008-0033-5.
[17] Ganguli A, Rappaport CM, Abramo D, Wadia-Fascetti S. Synthetic aperture imaging for flaw detection in a concrete medium. NDT E Int 2012 Jan 1;45(1):79–90. https://doi.org/10.1016/j.ndteint.2011.09.004.
[18] Hoegh K, Khazanovich L, Yu H. Ultrasonic tomography for evaluation of concrete pavements. Transport Res Rec: Journal of the Transportation Research Board 2011 Nov;10(2232):85–94. https://doi.org/10.3141/2232-09.
[19] Özdemir C, Demirci Ş, Yiğit E, Yilmaz B. A review on migration methods in B-scan ground penetrating radar imaging. Math Probl Eng 2014:2014. https://doi.org/10.1155/2014/280738.
[20] Hugenschmidt J, Kalogeropoulos A, Soldovieri F, Prisco G. Processing strategies for high-resolution GPR concrete inspections. NDT E Int 2010 Jun 1;43(4):334–42. https://doi.org/10.1016/j.ndteint.2010.02.002.
[21] Gucunski N, Rascoe C, Maher A. 3d-GPR in transportation infrastructure evaluation. In21st EEGS symposium on the application of geophysics to engineering and environmental problems. 2008 Apr 6.
[22] Wang ZW, Zhou M, Slabaugh GG, Zhai J, Fang T. Automatic detection of bridge deck condition from ground penetrating radar images. IEEE Trans Autom Sci Eng 2011;8(3):633–40. https://doi.org/10.1109/TASE.2010.2092428.
[23] Kaur P, Dana KJ, Romero FA, Gucunski N. Automated GPR rebar analysis for robotic bridge deck evaluation. IEEE transactions on cybernetics 2016;46(10):2265–76. https://doi.org/10.1109/TCYB.2015.2474747.
[24] Dinh K, Gucunski N, Duong TH. An algorithm for automatic localization and detection of rebars from GPR data of concrete bridge decks. Autom ConStruct 2018;89:292–8. https://doi.org/10.1016/j.autcon.2018.02.017.
[25] Dinh K, Gucunski N, Duong TH. Migration-based automated rebar picking for condition assessment of concrete bridge decks with ground penetrating radar. NDT E Int 2018;98:45–54. https://doi.org/10.1016/j.ndteint.2018.04.009.
[26] Yelf R. Where is true time zero? Ground Penetrating Radar. GPR 2004. Proceedings of the tenth international conference on (vol. 1, pp. 279–282). IEEE; 2004. 2004.
[27] Khan US, Al-Nuaimy W. Background removal from GPR data using eigenvalues. InGround Penetrating Radar (GPR). 13th international conference on 2010 Jun 21 IEEE; 2010. p. 1–5. https://doi.org/10.1109/ICGPR.2010.5550079.
[28] Kim JH, Cho SJ, Yi MJ. Removal of ringing noise in GPR data by signal processing. Geosci J 2007 Mar 1;11(1):75–81. https://doi.org/10.1007/BF02910382.
[29] Glass GK, Buenfeld NR. The presentation of the chloride threshold level for corrosion of steel in concrete. Corrosion Sci 1997 May 1;39(5):1001–13. https://doi.org/10.1016/S0010-938X(97)00009-7.
[30] Pailes BM, Gucunski N. Understanding multi-modal non-destructive testing data through the evaluation of twelve deteriorating reinforced concrete bridge decks. J Nondestr Eval 2015 Dec 1;34(4):30. https://doi.org/10.1007/s10921-015-0308-6.